Journal of Visualization, Vol. 9, No. 3 (2006)291-299

Topological Flow Characteristics in a Butterfly Valve Used for a Spark Ignition Engine

Kim, S.[*1], Kim, J.[*1], Choi, J.[*1] and Sung, J.[*2]

*1 School of Mechanical and Aerospace Engineering, College of Engineering, Sunchon National University, Suncheon, Jeonnam 540-742, Korea. E-mail: ksc@sunchon.ac.kr
*2 Department of Mechanical Engineering, School of Manufacturing Engineering, Seoul National University of Technology, Seoul 139-743, Korea.

Received 8 October 2005
Revised 11 January 2006

Abstract : The flow fields in a butterfly valve, consisting of a circular cylinder and a circular plate with a circular shaft, are numerically investigated with changing the valve angle, i.e., 15°, 45°, 75° and 90°(full-open). The corresponding Reynolds numbers are chosen as 10^4, 4×10^4, 7×10^4, and 10^5. The pressure drops between the entrance and the exit of the valve are 0.904, 0.575, 0.382 and 0.199, respectively at the above four valve positions. The moment coefficients calculated for the valve shaft are mostly due to the unbalanced pressure distribution on the both sides of the valve plate and -0.365, -0.082, -0.033 and 0, respectively, for each valve angle. The pressure distribution on the valve cylinder and the topological streamline patterns qualitatively show the flow field exceedingly agitated by the valve plate and its shaft.

Keywords : Butterfly valve, Blockage ratio, Pressure drop, Moment coefficient.

1. Introduction

A butterfly valve, also called a throttle valve, has been used to control the flow rate for a while and it has a lot of advantages such as good reliability, easy controllability and simple geometry and so on. It is adequate to block or to throttle the internal flow effectively, able to treat much flow rate in the relatively low pressure, and also works well when the fluid is contaminated more or less. It consists of an outer circular cylinder and circular plate which is operated within 90° by a rotational shaft and has the small inertia to run swiftly. By these positive reasons, it is widely used in the SI (spark ignition) gasoline engine for the control of the intake air flow rate in the wide range, pipeline and chemical plant, etc. However, the flow characteristics inside a butterfly valve have not been investigated precisely. The schematic flow field inside a butterfly valve is described as follows; upstream stagnation region in the front lower plate, a kind of wall jet between the valve plate and the outer cylinder, separated recirculation zone on the upper valve plate and in the downstream, and merged flows of wall jet and separated flow. (Eom, 1998) So the flow field inside a throttle valve is generally highly complicated.

Recently, there have been a lot of researches for combustor geometry, combustion method, air-fuel mixing, fuel supply, and exhaust gas treatment in order to improve the fuel-consumption rate and to develop the clean technology in the gasoline engine. Since air flow incoming into an engine passes through air-filter, throttle valve, intake manifold and intake valve in series, this intake

system has an influence on the grain size of fuel droplet, swirl and tumble which are directly related to combustion phenomena. Generally, fuel is optimally injected according to the opening angle of a throttle valve which is operated due to the engine load. When the valve angle is small, i.e., the blockage ratio is large, the large recirculation region will form behind a valve plate, and thus large pressure drop will occur. For the remedy, arrays of small holes on the valve plate could reduce the pressure loss and increase the air-fuel mixing. Most of modern gasoline engines adopt the multipoint injection, and the gasoline direct injection method like a diesel engine is applied recently. In the traditional driving condition with the valve angle of 20°~45° except the full-opening, more than 90% of the total intake pressure loss would occur through the throttle valve passage.

Obata et al. (1993) numerically calculated the loss coefficient for several valve angles around a two-dimensional butterfly valve, and Huang and Kim (1996) analyzed three-dimensional incompressible flow inside a butterfly valve using a commercial code. In general, it is relatively complicated and not so easy to analyze the flow field in the intake system which consists of several devices. Especially, the most difficult work is to generate grid system inside a valve, since the external and internal flow field seems to be mixed in the view of grid generation and physics of flow. Until now, the most researches on the throttle valve have focused on the pressure loss due to the valve and the characteristics of flow control (Eom, 1988; Addy et al. 1985; Morris and Dutton, 1989, 1991; Caille and Laumonier, 1998), however few papers are found which investigate the general flow field according to the valve opening angles. Thus, in this paper the flow field inside a throttle valve used for a SI engine is computed numerically for several opening angles of the valve plate.

2. Numerical Analysis

The Navier-Stokes equation has one of elliptic, parabolic and hyperbolic types depending on the flow states, i.e., incompressible or compressible. The pressure term needs to be treated specially and can be considered as a dynamic parameter in the governing equation. If the artificial compressibility is introduced to reduce the computational time required to obtain the divergence free condition, the steady incompressible Navier-Stokes equations can be solved effectively in similar ways adopted in the compressible flow solver.

Now the continuity equation is modified by adding the time derivative of pressure based on the artificial compressibility concept as below to result in a hyperbolic system.

$$\frac{1}{\beta}\frac{\partial p}{\partial t}+\frac{\partial u_i}{\partial x_i}=0 \tag{1}$$

where p is the pressure, u_i the velocity vector, t the time, x_i the coordinate and β the artificial compressibility constant and should be chosen according to a Reynolds number and characteristic length of the geometry through the wave propagation analysis. And using with the time-averaged primitive variables and constant density, the Navier-Stokes equation becomes

$$\frac{\partial u_i}{\partial t}+\frac{\partial u_i u_j}{\partial x_j}=\frac{1}{\rho}\left[-\frac{\partial p}{\partial x_i}+\frac{\partial \tau_{ij}}{\partial x_j}\right] \tag{2}$$

where ρ is the fluid density and τ_{ij} the viscous stress tensor.

By nondimensionalizing all of the physical variables by a reference velocity and length, the combination of Eqs. (1) and (2) has the conservative form of

$$\frac{\partial D}{\partial t}+\sum_{i=1}^{3}\frac{\partial (F_i-F_{vi})}{\partial x_i}=0 \tag{3}$$

where

$$D=\begin{bmatrix} p \\ u \\ v \\ w \end{bmatrix},\quad [F_i]=\begin{bmatrix} \beta u_i \\ uu_i+\delta_{1i}p \\ vu_i+\delta_{2i}p \\ wu_i+\delta_{3i}p \end{bmatrix},\quad [F_{vi}]=\begin{bmatrix} 0 \\ \tau_{1i} \\ \tau_{2i} \\ \tau_{3i} \end{bmatrix},\ \delta_{ki}\ : \text{the Kronecker delta.}$$

In order to calculate the general three-dimensional flow field around an arbitrary geometry, it

is necessary to transform the physical coordinates into the general curvilinear ones; $\tau = t$, $\xi_i = \xi_i(x,y,z)$, $\xi_{i_{x_i}} = J(x_{j_{\xi_j}} x_{k_{\xi_k}} - x_{j_{\xi_k}} x_{k_{\xi_j}})$, etc, where J is the Jacobian of the transformation. Thus the final difference form of the conservative Eq. (3) becomes

$$\delta_\tau \hat{D} + \sum_{i=1}^{3} \delta_{\xi_i} (\hat{F}_i - \hat{F}_{vi}) = 0 \tag{4}$$

where $\hat{}$ means the vectors in transformed coordinates and δ the finite difference and

$\hat{D} = J^{-1} D$, $\hat{F}_i = J^{-1}[(\xi_i)_t D + \sum_j (\xi_i)_{x_j} F_j]$, $\hat{F}_{vi} = J^{-1} \sum_j (\xi_i)_{x_j} F_{vj}$.

Eq. (4) can be solved by the implicit, noniterative, approximately factorized and finite difference scheme. The difference for time with second order accuracy is expressed by the trapezoidal rule (Beam and Warming, 1976)

$$\delta_\tau \hat{D} = \frac{1}{2}(\delta_\tau \hat{D}^{n+1} + \delta_\tau \hat{D}^n) + O(\Delta\tau^2) \tag{5}$$

where the superscript n and $n+1$ mean the time step and $\Delta\tau$ is its size. The convected flux vectors which are the nonlinear function should be locally linearized using the Taylor series expansion (Chang and Kwak, 1984).

$$\hat{F}_i^{n+1} = \hat{F}_i + \frac{\partial \hat{F}_i^n}{\partial \hat{D}} (\hat{D}^{n+1} - \hat{D}^n) + O(\Delta\tau^2), \tag{6}$$

where $\partial \hat{F}_i / \partial \hat{D}$ is the Jacobian matrices and denoted by $\hat{A}_i$ from now on. To write the viscous flux vector as the function of the physical variables vector, it is assumed that the coordinate system is orthogonal, viscosity is constant and the velocity field is divergence-free, then

$$\hat{F}_{vi} = (\nu + \nu_t) J^{-1} \nabla \xi_i \cdot \nabla \xi_i \tilde{I} \frac{\partial \hat{D}^{n+1}}{\partial \xi_i} = \Gamma_i \hat{D}^{n+1} \tag{7}$$

where $\tilde{I} = [i_{ij}]$, $i_{ij} = \delta_{ij}$, and $i_{11} = 0$.

The Jacobian matrix defined above is finally rearranged as

$$\hat{A}_i = \frac{1}{J} \begin{bmatrix} L_0 & L_1\beta & L_2\beta & L_3\beta \\ L_1 & Q_i + L_1 u & L_2 u & L_3 u \\ L_2 & L_1 v & Q_i + L_2 v & L_3 v \\ L_3 & L_1 w & L_2 w & Q_i + L_3 w \end{bmatrix}$$

where Q is the contravariant velocity, L_0 the grid speed and L_j the metrics, i.e., $Q_i = L_0 + \sum_j L_j u_j$, and $L_0 = (\xi_i)_t$, $L_j = (\xi_i)_{x_j}$. Substituting Eqs. (5) and (6) into Eq. (4), the linearized system in delta form can be obtained,

$$\left[I + \frac{h}{2} J^{n+1} \sum_i \delta_{\xi_i} (\hat{A}_i^n - \Gamma_i) \right] (\hat{D}^{n+1} - \hat{D}^n) = -\Delta\tau J^{n+1} \left[\sum_i \delta_{\xi_i} (\hat{F}_i - \hat{F}_{vi})^n \right] + \left(\frac{J^{n+1}}{J^n} - 1 \right) = RHS \tag{8}$$

where $h = \Delta\tau$ (trapezoidal scheme), or $2\Delta\tau$ (Euler's scheme).

Since it is very difficult to solve Eq. (8) directly, approximate factorization scheme is adopted, i.e., Eq. (8) can be splitted to use a multi-stage one-dimensional inversion scheme such as ADI(alternating direction implicit) method, which can be effectively solved by the well-known Thomas algorithm. Thus Eq. (8) is approximately factorized with second order central differencing and finally comes to get the 3 block tridiagonal matrices. That is, Eq. (9) can be solved through three-stage ADI method using a block LU(lower-upper triangular) decomposition procedure.

$$\prod_{i=1}^{3} L_{\xi_i} (\hat{D}^{n+1} - \hat{D}^n) = RHS \tag{9}$$

where $L_{\xi_i} = \left[I + \frac{\Delta\tau}{2} J^{n+1} \delta_{\xi_i} (\hat{A}_i^n - \Gamma_i) \right]$, and I is a unit matrix.

It is necessary to introduce the diagonal algorithm in order to solve Eq. (9) more efficiently with the reduced calculation time, which diagonalizes the Jacobian matrices into the similarity form and converts Eq. (9) into the uncoupled one (Pulliam and Chaussee, 1981). The block tridiagonal matrices are changed to the scalar ones, and there is a similarity transformation which makes the Jacobian

matrices to be diagonalized such as $\hat{A}_i = T_i \hat{\Lambda}_i T_i^{-1}$, where $\hat{\Lambda}_i$ is a diagonal matrices consisting of the eigenvectors T_i of the Jacobian matrices, i.e.,

$$\hat{\Lambda}_i = \frac{1}{J}\begin{bmatrix} Q_i & 0 & 0 & 0 \\ 0 & Q_i & 0 & 0 \\ 0 & 0 & Q_i + C_i & 0 \\ 0 & 0 & 0 & Q_i - C_i \end{bmatrix}$$

and C_i is the pseudo-speed of sound defined by $C_i = \sqrt{(Q_i - L_0)^2 + \beta \Sigma_j L_j^2}$ due to the artificial compressibility. T_i is derived in detail by Pullian and Chaussee (1981), and its determinant is a function of a kind of pseudo-speed of sound. The linear, implicit and differential operator is changed to the following form in a similar ways applied to the Jacobian matrices.

$$L_{\xi_i} = T_{\xi_i}\left[I + \frac{\Delta\tau}{2} J \delta_{\xi_i} (\hat{\Lambda}_i - \hat{\Gamma}_i) \right] T_{\xi_i}^{-1}$$

where $\hat{\Gamma}_i = (\nu + \nu_t) J^{-1} \nabla\xi_i \cdot \nabla\xi_i I \delta_{\xi_i}$.

Meanwhile, the implicit approximate factorization and diagonalization algorithm make the solution unstable due to the higher order oscillations because the second-order central differencing is used for the space. These phenomena are serious in the calculation of high Reynolds number flows. Generally, the second- or fourth-order artificial dissipation (or smoothing) term should be added to Eq. (9) to dissipate the undesirable oscillation. Thus RHS in Eq. (9) and the differencing operator are modified respectively by introducing the numerical dissipation.

$$RHS \rightarrow RHS - \varepsilon_E [\sum(\nabla_{\xi_i} \Delta_{\xi_i}^2)] \hat{D}^n, \quad L_{\xi_i} = \left[I + \frac{\Delta\tau}{2} J^{n+1} \delta_{\xi_i} (\hat{A}_i^n - \Gamma_i) - \varepsilon_I \nabla_{\xi_i} \Delta_{\xi_i} \right],$$

where ε_E and ε_I are the smoothing coefficients depending on the Reynolds number and grid size (Chang and Kwak, 1984).

The viscous stress tensor in Eq. (2) is modeled by the Baldwin-Barth turbulence model (Baldwin and Barth, 1991) which is a kind of one-equation model. This model includes seven closure coefficients, two empirical damping functions and a function describing the turbulence length scale, and it is summarized as follows. The kinematic eddy viscosity is

$$\nu_t = C_\mu \nu \tilde{R}_t D_1 D_2,$$

where

$$\frac{\partial}{\partial t}(\nu\tilde{R}_t) + U_j \frac{\partial}{\partial x_j}(\nu\tilde{R}_t) = (C_{\varepsilon 2} f - C_{\varepsilon 1})\sqrt{\nu\tilde{R}_t \phi} + \left(\nu + \frac{\nu_t}{\sigma_\varepsilon}\right)\frac{\partial^2 \nu\tilde{R}_t}{\partial x_k \partial x_k} - \frac{1}{\sigma_\varepsilon}\frac{\partial \nu_t}{\partial x_k}\frac{\partial \nu\tilde{R}_t}{\partial x_k},$$

$$\phi = \nu_t \left[\left(\frac{\partial U_i}{\partial x_j} + \frac{\partial U_j}{\partial x_i} \right) \frac{\partial U_i}{\partial x_j} - \frac{2}{3}\left(\frac{\partial U_k}{\partial x_k} \right)^2 \right], \; U_i \text{ is mean velocity}, \; D_1 = 1 - e^{-y^+/A_0^+}, \; D_2 = 1 - e^{-y^+/A_2^+},$$

$$f = \frac{C_{\varepsilon 1}}{C_{\varepsilon 2}} + \left(1 - \frac{C_{\varepsilon 1}}{C_{\varepsilon 2}}\right)\left(\frac{1}{\kappa y^+} + D_1 D_2\right)\left[\sqrt{D_1 D_2} + \frac{y^+}{\sqrt{D_1 D_2}}\left(\frac{D_2}{A_0^+} e^{-y^+/A_0^+} + \frac{D_1}{A_2^+} e^{-y^+/A_2^+}\right)\right],$$

$C_{\varepsilon 1} = 1.2$, $C_{\varepsilon 2} = 2.0$, $C_\mu = 0.09$, $A_0^+ = 26$, $A_2^+ = 10$, $\kappa = 0.41$, and $\sigma_\varepsilon = \kappa^2 [(C_{\varepsilon 2} - C_{\varepsilon 1})\sqrt{C_\mu}]^{-1}$.

No-slip boundary conditions are applied on the solid surface or walls. Constant total pressure and uniform velocity are initially set on the inflow boundary surface. On the outflow boundary, the velocity is extrapolated and uniform constant static pressure is initially set. The pressures on both the inlet and the exit are changed during the every computational step.

The grid systems for a real throttle valve (Fig. 1) used for a passenger car consist of two blocks and are generated using the GENIE++ (Soni et al., 1992). The diameters of the outer cylinder, the circular valve plate, and the valve shaft are 50 mm, 50 mm and 10 mm, respectively. The total length of the cylinder is taken as twelve times of the cylinder diameter, i.e., $|x/D| \leq 6$ where the x-axis is taken as the main flow direction and consistent with the center line of the valve cylinder. The z-axis is the center line of the valve shaft. Figure 2 shows a sample grid generation for the 45° valve angle.

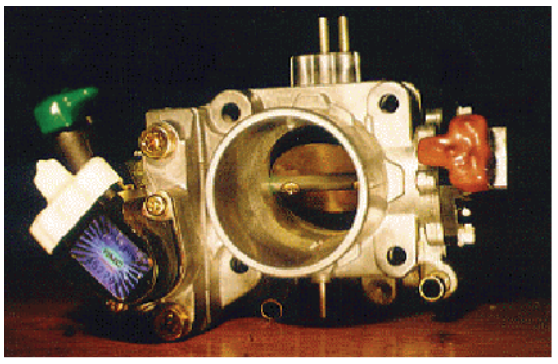

Fig. 1. A throttle body used for a passenger car.

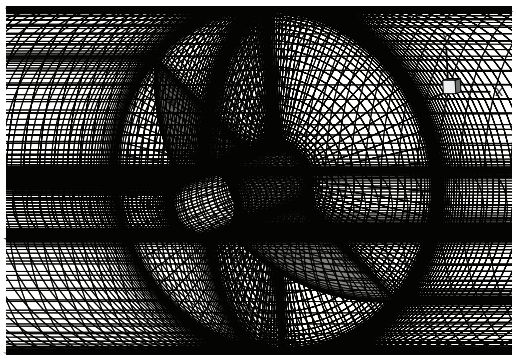

Fig. 2. Typical grid generation for the valve angle of 45°.

3. Results and Discussion

The circular disk valve is operated by a shaft in the range from 0° (fully closed) to 90° (fully open) inside a circular cylinder. The computation is executed for four valve angles and the basic conditions are given in Table 1, where the pressure-drop coefficient defined by $\Delta C_p = (p_{inlet} - p_{exit}) / p_{inlet}$ and the moment coefficient for the valve shaft defined by $C_M = moment/(0.5\rho U_\infty^2 AR)$ are calculated based on the computational results. Here, ρ is the density of air, U_∞ the inlet mean velocity, A the valve disk area and R the valve disk radius. The pressure mainly contributes the moment and thus the friction acting on the surface is neglected. The moment is calculated by $\int rpdA$ on the upper and lower surfaces of the valve plate. The coefficients are also listed in Table 1. The blockage ratio is constant of 0.22 due to the valve shaft when the valve angle is greater than 80°. The pressure loss increases severely and the moment clockwise acting on the shaft becomes steeply large as the valve angle decreases. The moment exerting on the valve shaft is more important to control the valve position accurately when the valve is open slightly.

Table 1. Computational conditions, and pressure-drop and moment coefficients.

Valve Angle (°)	Reynolds number	U_∞ (m/s)	Blockage Ratio (%)	ΔC_p	C_M
15	10,000	2.6	99.6	0.904	-0.365
45	40,000	10.4	70.7	0.575	-0.082
75	70,000	18.2	25.8	0.382	-0.033
90	100,000	26	22.0	0.199	0

Figure 3 depicts the flow passage observed from the front of the valve. The flow field in a butterfly valve is highly complicated due to the valve plate and shaft which might be considered as a kind of obstacles in the internal flow. Figures 4-7 show the pressure distribution around the valve plate. At 15°, the flow field is blocked very much, and thus there is lots of pressure difference before and after the valve plate. Pressure near the entrance of the valve cylinder reduces rapidly and it becomes strongly negative behind the valve plate. As the valve angle increases, i.e., the blockage ratio decreases, the downstream pressure is recovered and introduced toward the manifold. Especially, when the valve is fully open, the lowest pressure field is generated behind the valve shaft and the stagnated pressure is induced just before the valve shaft. From the pressure distribution on the cylinder surface, it can be figured out that the flow field will be highly complicated. That will be confirmed later from the view of the streamlines. As known from the legends in the surface pressure distributions, the differences between the maximum and minimum values of pressures increase as the valve angle increases. This means that there occurs relatively large pressure drop proportional to

the angles and results the high suction in the throttle valve. Since the minor loss is small due to the little blockage when the angle is large, however, the pressure is favorably recovered at the large valve angle. To reduce or remove the high pressure loss when the valve is slightly open, several small holes on the valve plate can be applied. (Eom, 1988; Lee et al., 1996).

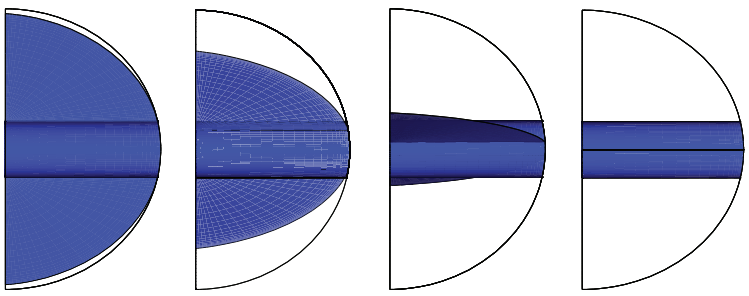

Fig. 3. Flow passage observed from the valve entrance (15°, 45°, 75° and 90° from left).

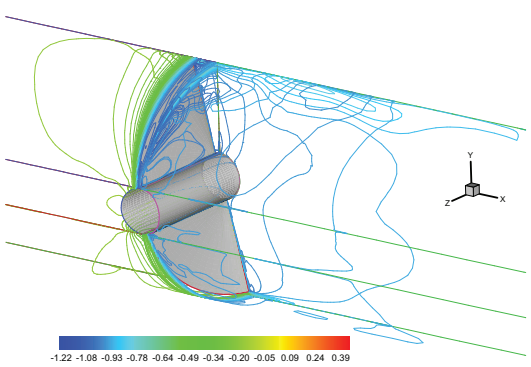

Fig. 4. Pressure contour at 15°.

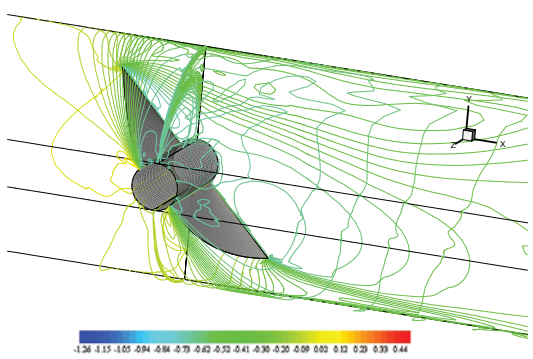

Fig. 5. Pressure contour at 45°.

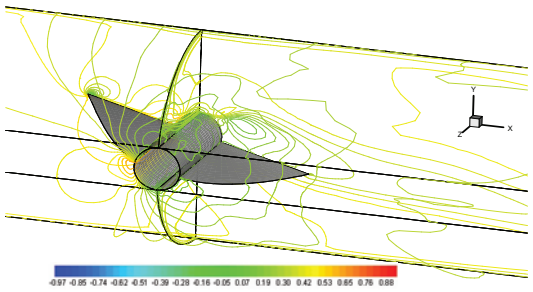

Fig. 6. Pressure contour at 75°.

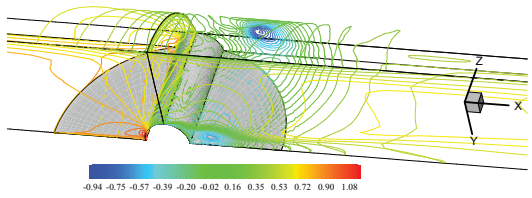

Fig. 7. Pressure contour at 90°.

The streamline patterns are topologically described in Figs. 8-11 according to the valve angles. The flow field behind the valve plate is very disturbed, and separates on the valve edges to generate the recirculation zone except the fully-open case. The valve plate plays a major role at the relatively small angle, and on the other hand the valve shaft is mostly related to make the flow filed complex. The downstream flow patterns get entangled and guided to the manifold except the fully open case in which the streamlines become complicated only near the valve shaft. Generally, there are evidences for the three-dimensional flow complexity such as spiral focus and saddle point. The highly entangled stream comes in effect to the severe pressure loss at the relatively low valve angle. Figure 12 shows the secondary flow patters at the valve exit. At 15°, a couple of weak and strong spiral

vortices are found, and a saddle locates just near the symmetric plane. When the valve angle increases, i.e. at 45° and 75°, single big vortex is generated except a tiny vortex formed at the upper top on the crossection. If the valve angle increases to reach the full open condition (90°), there exist four cells and two saddles. These strong secondary flows would be introduced to the engine cylinder and that would contribute to enhance the air-fuel mixing. In addition, the magnitude contours of the streamwise velocity are also depicted in Fig. 12 and the total velocity magnitudes are similarly distributed since the velocities in the direction of longitudinal and traverse directions are relatively very little to the streamwise velocity.

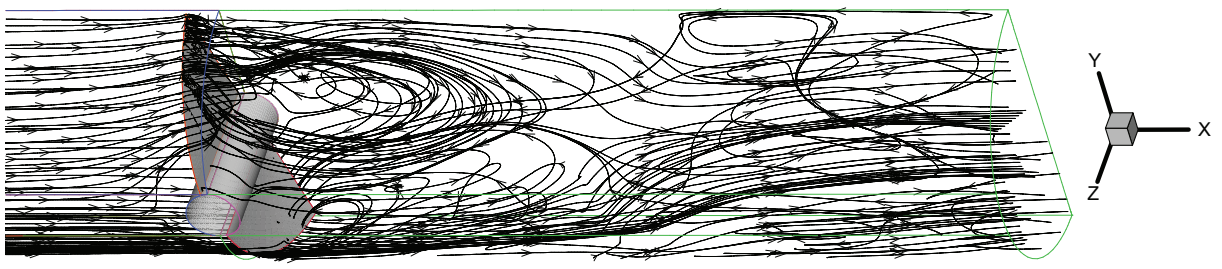

Fig. 8. Streamlines at the valve angle of 15°.

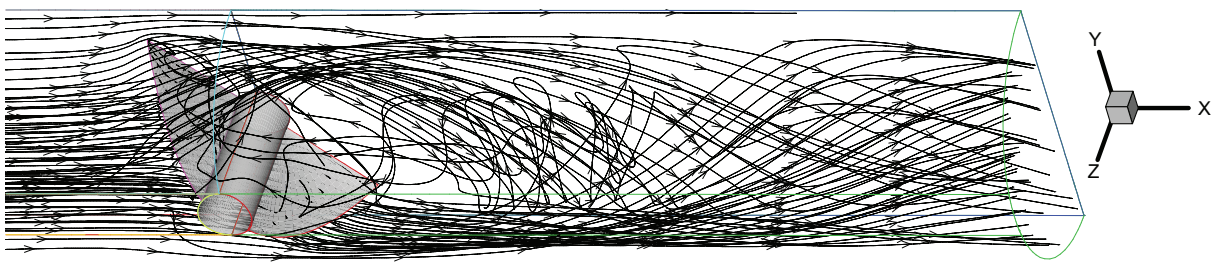

Fig. 9. Streamlines at the valve angle of 45°.

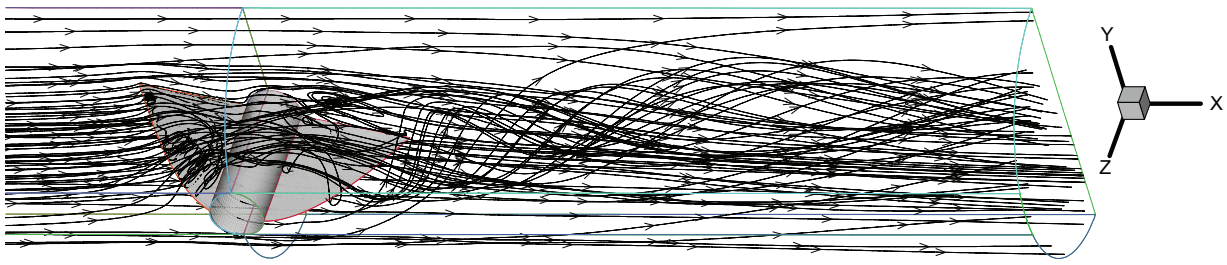

Fig. 10. Streamlines at the valve angle of 75°.

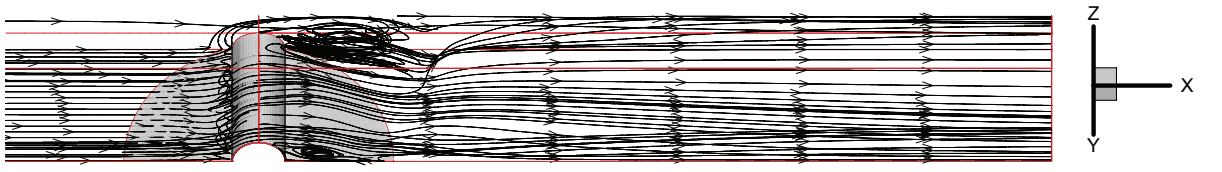

Fig. 11. Streamlines at the valve angle of 90°.

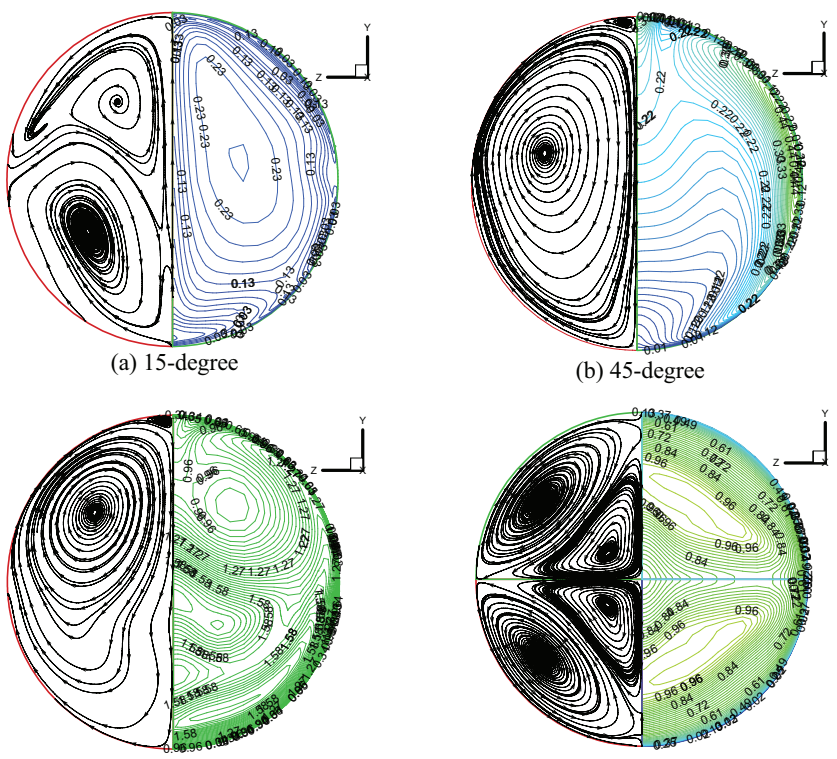

(a) 15-degree (b) 45-degree

(c) 75-degree (d) 90-degree

Fig. 12. Streamline patterns (left) and total velocity magnitude contours (right) at the exit.

4. Conclusion

This research investigates the topological flow characteristics in a butterfly valve for four valve opening angles. The large pressure drop and moment coefficient are caused from a great deal of the blockage ratio. The flow fields are highly complicated due to the valve plate and shaft and thus these induce the large flow loss. The flow field behind the valve plate is immensely agitated when the valve angles are relatively small. It is found that there are kinds of cell patterns on the plane of the valve exit; two cells at 15°, one cell at 45° and 75°, 4 cells at 90° on the half plane. They would improve the mixing rate of air and fuel in the engine cylinder in the view of the strong secondary flow phenomena

Acknowledgement

This work was supported by the NURI project of the Ministry of Education, Korea in 2005.

References

Addy, A. L., Morris, N. J. and Dutton, J. C., An Investigation of Compressible Flow through Butterfly Valves, ASME J. of Fluids Eng., 107 (1985), 512-517.

Baldwin, B. S. and Barth, T. J., A One-equation Turbulence Model for High Reynolds Number Wall-bounded Flows, AIAA Paper 91-0610 (1991), Reno, Nevada, USA.

Beam, R. M. and Warming, R. F., An implicit finite-difference algorithm for hyperbolic system in conservative-law form, J. Comp. Phys., 22 (1976), 87-110.

Caille, V. and Laumonier, J., Effect of Periodic Aerodynamic Pulsation on Flow over Confined Butterfly Valve, Experiments in Fluids, 25 (1998), 362-368.

Chang, J. L. and Kwak, D., On the Method of Pseudo-compressibility for Numerically Solving Incompressible Flows, AIAA Paper 84-0252 (1984).

Eom, K., Performance of Butterfly Valve as a Flow Controller, ASME J. of Fluids Eng., 110 (1988), 16-19.

Huang, C. and Kim, R. H., Three-dimensional analysis of Partially Open Butterfly Valve Flows, ASME I. of Fluids Eng., 118 (1996), 562-568.

Kim, S. and Soni, B. K., Steady 3D Incompressible Flow analysis for the Simplified Train-tunnel Interaction, Computer Assisted Mechanics and Engineering Sciences, 7-1 (2000), 23-37.
Lee, C. S. and Cho, B., A Study on the flow Characteristics of the Mixture in an Intake Manifold, The Korean Society of Automotive Engineers, 4-1 (1996), 218-228 (in Korean).
Lee, C. S., Lee, K. H., Cho, B. O. and Oh, K. S., A Study of the Secondary Atomization Characteristics of Liquid Fuel in the Perforated Throttle Valve, J. of ILASS-Korea, 1-1 (1996), 55-62 (in Korean).
Morris, M. J. and Dutton, J. C., Compressible Flowfield Characteristics of Butterfly Valves, ASME J. of Fluids Eng., 111 (1989), 400-407.
Morris, M. J. and Dutton, J. C., An Experimental Investigation of Butterfly Valve Performance Downstream of an Elbow, ASME J. of Fluids Eng., 113 (1991), 81-85.
Obata, M., Nakao, Y., Satofuka, N. and Morinish, K. Numerical Solution of 2-Dimensional Flows through Butterfly Valve Using Overset Grid Technique, J. of JSME, 59-562, B (1993), 1994-2000.
Pulliam, T. H. and Chaussee, D. S., A diagonal Form of an Implicit Approximate-factorization Algorithm, J. Comp. Phys. 39 (1981), 347-363.
Soni, B. K., Thompson, J. F., Stokes, M. and Shih, M.-S., GENIE++, EAGLEView and TIGER: General and Special Purpose Interactive Grid Systems, AIAA Paper 92-0071 (1992).

Author Profile

Sungcho Kim: He received his master and Ph.D. degrees in Aeronautical Engineering in 1985 and 1989, respectively from KAIST, Korea, and worked in Central Technology Institute of Daewoo Heavy Industry Ltd. He researched in Mississippi State University and University of California, Santa Barbara as a visiting scholar in 1994 and 2000, respectively. And he served as the dean in college of engineering, Sunchon National University, and has been working in school of mechanical and aerospace engineering in Sunchon National University as a professor since 1989. His research area is experimental and computational fluid engineering.

Jeong Soo Kim: He received his master and Ph.D. degrees in Aeronautical Engineering in 1987 and 1992, respectively from KAIST, Korea, and was with in KIMM, ADD, and KARI as a senior researcher. Also he researched in TRW(USA) as an assistant program manager from 1996 to 1998. And he has been a faculty member in school of mechanical and aerospace engineering in Sunchon National University since 2004. His research interests are satellite propulsion system, measurement and visualization of injector spray pattern using PDA, combustion, test and evaluation of liquid rocket engine, etc.

Jonwook Choi: He received his master and Ph.D. degrees in Mechanical Engineering in 1995 and 1999, respectively from Chonnam National University, Korea, and worked for POSCO Technology Research Laboratories as a Post-doctoral researcher. Also he taught in mechanical and automotive engineering of Sunchon National University as a contract professor for four years. And he has been working in school of mechanical and aerospace engineering in Sunchon National University as a professor since 2005. His research interests are heat transfer, computational fluid dynamics, etc.

Jaeyong Sung: He received his master and Ph.D. degrees in Mechanical Engineering in 1996 and 2001, respectively from Seoul National University, Korea, and was with Digital Appliance Laboratory of LG Electronics Inc. as a senior researcher. Also he taught in mechanical and automotive engineering of Sunchon National University as a professor. And he has been working in school of manufacturing engineering in Seoul National University of Technology as a professor since 2004. His research interests are all the areas related to PIV technology, hemodynamics, biochips, rarefied gas flow with DSMC, etc.